Sensors and Actuators A 197 (2013) 30–37

Contents lists available at SciVerse ScienceDirect

Sensors and Actuators A: Physical

journal homepage: www.elsevier.com/locate/sna

Wireless LTCC-based capacitive pressure sensor for harsh environment

Jijun Xiong[a], Ying Li[a], Yingping Hong[a], Binzhen Zhang[a], Tianhong Cui[b], Qiulin Tan[a], Shijun Zheng[a], Ting Liang[a,*]

[a] National Key Laboratory for Electronic Measurement Technology, North University of China, No. 3 Xueyuan Road, Taiyuan 030051, Shanxi, China
[b] Department of Mechanical Engineering, University of Minnesota Twin Cities, USA

ARTICLE INFO

Article history:
Received 18 July 2012
Received in revised form 28 February 2013
Accepted 2 April 2013
Available online 8 April 2013

Keywords:
Capacitive pressure sensor
Wireless
Low temperature co-fired ceramic (LTCC)
Harsh environment
Sacrifice paste

ABSTRACT

This paper presents a wireless capacitive pressure sensor based on LTCC (low temperature co-fired ceramic) technology, where the design, fabrication, and measurement of the sensor is demonstrated and discussed. Differ from traditional LTCC process flow, a unique process of screen-printing sacrifice layer has been introduced to avoid deformation of the capacitive embedded cavity during lamination or sintering, which leads to a better performance of the sensor. A greater sensitivity of the sensor, comparing with its predecessors, is showed during measurement. Finally ways for future optimization are proposed.

© 2013 Elsevier B.V. All rights reserved.

1. Introduction

In recent years, LTCC is widely used in applications like RF circuits, microwave device, package, etc., when referring to MEMS structures like pressure sensor, especially capacitive pressure sensor, seldom have we seen the usage of LTCC. As traditional pressure sensors, mostly made from micro machining silicon, show great limitation when exposed to harsh environment like high temperature circumstances, LTCC, which operates arbitrarily well at 400–600 °C with perfect dielectric and chemical-proof characters, seems to be a relatively qualified substitute. The easy-machining of every single green tape, the favorable integrity of different layers after co-firing and the compatibility with thick-film technology make LTCC technology show apparent superiority over some other heat-resistant materials, especially in the fabrication process of capacitive pressure sensor which includes the forming of an embedded cavity [1–10].

Prof. Mark. G. Allen's team from Georgia Tech. had been committing to the research of the wireless high temperature ceramic pressure sensor since 1998 [1–4], with the debut of the MEMS 'Sandwich' structure, they pioneered and developed the technology of LTCC wireless capacitive pressure sensor, the sensitivity of their sensors reaches 150 kHz/bar around.

Another research team in Novi Sad, Serbia, published improved model in 2009 [5,6], which demonstrates a better structure but worse performance compared to the prior. Two extra LTCC layers are laminated above the metal pattern, which provides a perfect protection of the exposed circuit, but their sensor's sensitivity is only 25.6 kHz/bar.

In this work, a wireless capacitive pressure sensor for harsh environment based on LTCC technology is realized. A LC resonant circuit is employed to detect the variation of the sensor's frequency caused by the pressure applied, and the measurement of pressure can be translated to that of sensor's frequency, which can be detected remotely, using the coupling theory.

Differ from the previous structure, a new square capacitive cavity structure is designed, the key technology in the fabrication of the embedded cavity, the sacrifice paste, is firstly introduced into this MEMS (micro electromechanical system) structure. More favorable membrane flatness is realized for the improvement of sensor's sensitivity, which provides the sensor an overwhelming advantage of high precise pressure measurement over the previous LTCC capacitive sensors

2. Design and fabrication

A schematic of the sensor is presented in Fig. 1, from which we can see that the structure consists of three sections in general: top, middle and bottom section, the top section includes two layers of

* Corresponding author. Tel.: +86 0351 3921882; fax: +86 0351 3922131.
E-mail addresses: xiongjijun@nuc.edu.cn (J. Xiong), jelly_mage@163.com (Y. Li), hyp220@126.com (Y. Hong), zhangbinzhen@nuc.edu.cn (B. Zhang), tcui@me.umm.edu (T. Cui), tanqiulin.99@163.com (Q. Tan), zhengshijun2008@163.com (S. Zheng), liangtingpdf@163.com (T. Liang).

0924-4247/$ – see front matter © 2013 Elsevier B.V. All rights reserved.
http://dx.doi.org/10.1016/j.sna.2013.04.007

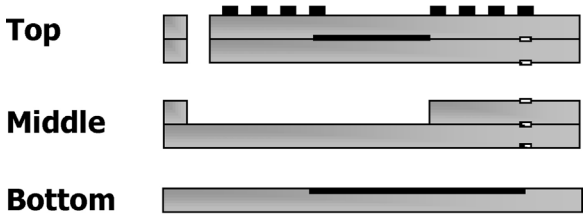

Fig. 1. Three sections of the sensor.

LTCC tape with square inductor coil on the surface of upper layer and square capacitor electrode on that of the beneath, a air gap hole is drilled near the left boundary of the layers; the middle section comprises two layers of LTCC tape, where an embedded cavity connected to an air channel is curved in the upper layer; the bottom section is made of one single layer where the lower capacitor electrode resides. The inductor coil and capacitor electrodes are connected through via across the layers.

From the cross-section view of the sensor in Fig. 2, we can make a simple functional analysis of the structure; to start with, the classical expression where the resonant frequency f_0 can be retrieved from:

$$f_0 = \frac{1}{2\pi\sqrt{L_s C_s}} \quad (1)$$

where L_s and C_s are the inductance and capacitance of the sensor, in ideal assumption, any variation of capacitance or inductance will lead to a shift of the resonant frequency, as for capacitive pressure sensors, whose inductance L_s, is a constant value (ideal situation), variation of pressure P will result in change of capacitor C_s, then shift of resonant frequency f_0, so the measurement of pressure variation will be translated into that of the sensor's resonant frequency shift f_0. In this five-layer structure, the two-layer-thick tapes above and below the embedded cavity served as membranes sensitive to pressure applied; the inner coil of inductor in layer 1 is connected to the upper capacitor electrode in layer 2 through via, and the outer coil to lower electrode in layer 5, forming a LC resonant circuit; the air-gap in layer 3 is used for releasing the pressure from the heated gas from the embedded cavity during co-firing.

The parameter of the sensor is demonstrated in Table 1.

The sensor is fabricated in traditional LTCC technology which covers shaping of green tapes, screen-printing of circuit pattern, stacking, laminating and co-firing of the structure. We use Dupont 951AT ceramic tapes for experiment, whose characteristics are shown in Table 2, Dupont Ag paste, whose CTE and shrinkage rate are relatively similar with the tapes, is used to make sure of a precise alignment. The tapes are firstly structured and hole-drilled through laser machining system; circuit pattern, interconnection are then screen-printed and via stencil-printed.

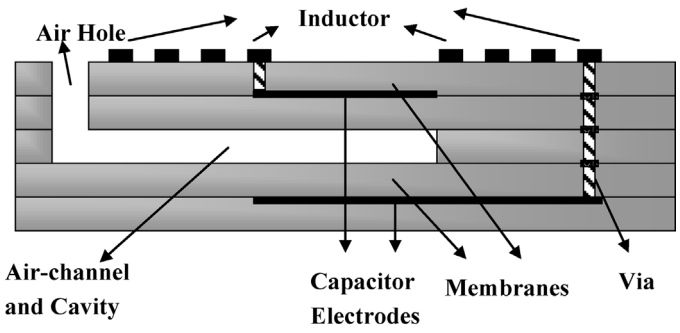

Fig. 2. Cross-section of the sensor.

Table 1
Parameters of the sensor designed.

Parameters	Value
Overall dimension	26 mm × 26 mm × 0.5 mm
Capacitor metal dimension	7 mm × 7 mm
Height of the embedded cavity	100 μm
Diameter of inner inductor coil	8.5 mm
Diameter of outer inductor coil	20 mm
Number of coil turns	18
Width of the coil	0.15 mm
Distance between neighbor coils	0.15 mm
Width of the interconnection	0.2 mm
Thickness of the printed pattern	12 μm
Via dimension	0.2 mm × 0.2 mm
Air channel dimension	8.5 mm × 0.5 mm
Air-hole dimension	0.5 mm × 0.5 mm

The sacrifice paste, which is applied to realize a favorable appearance, is also screen-printed into the cavity after the bottom and middle sections are laminated together. To meet our requirement, we made the paste from carbon particles and organic solvent [10,11], it would provide a strong support on the membrane above the cavity to avoid the membrane's collapse or even rupture during lamination and then volatize during co-firing, which is of great importance especially when the membrane's defection during lamination cannot been omitted compared with the thickness of LTCC tape, as the defection would sharply affect the sensor's sensitivity, measure range and accuracy in that case. Meanwhile, with the introducing of the sacrifice paste, a thinner membrane and cavity thickness can be attained, which can significantly improve the sensor's sensitivity.

Fig. 3 is the comparison of finished sensor samples with and without sacrifice paste, measured by Cyber Technologies Vantage50 thickness tester, from which we can clearly see the great role the sacrifice paste played in improving the cavity's quality, the sample without sacrifice paste stuffed has a collapse of about 20 μm in the center while that with only 8 μm around.

After the sacrifice paste process, we laminate all the three sections together and put the stack into the furnace for co-firing: 0–400 °C 5 h to volatize the organic particles, the 400–600 °C range, which is the crucial time for the cavity formation as both the sacrificial carbon material begins to burn out and the green tape starts to harden around 500 °C, would last a little bit longer about 6 h, 5 h from 600–900 °C and then 900–0 °C for 3 h. Finally, the air-hole is sealed with ESL 4774-BCG glass frit and the sample is put into furnace again for sintering of the glass frit, 0–700 °C for 1 h. The whole process flow is shown in Fig. 4.

Fig. 5a is the completed sensor sample, Fig. 5b is the SEM image of the surface inductor coils and Fig. 5c is the X-ray (DAGE XD7600NT) images of the 3D sensor sample structure.

3. Modeling

As what the simple analysis mentions above, the pressure P loaded creates the deflection d of the sensor's membrane, and the deflection causes a variation of the capacitance, which finally

Table 2
Parameters of Dupont 951 ceramic tape [12].

Parameters	Value
Young's modulus	152 GPa
Poisson's ratio	0.17
Relative permittivity	7.8
Unfired thickness	114.3 μm
X, *Y* shrinkage	13%
Z shrinkage	15%
CTE	5.8 ppm/C

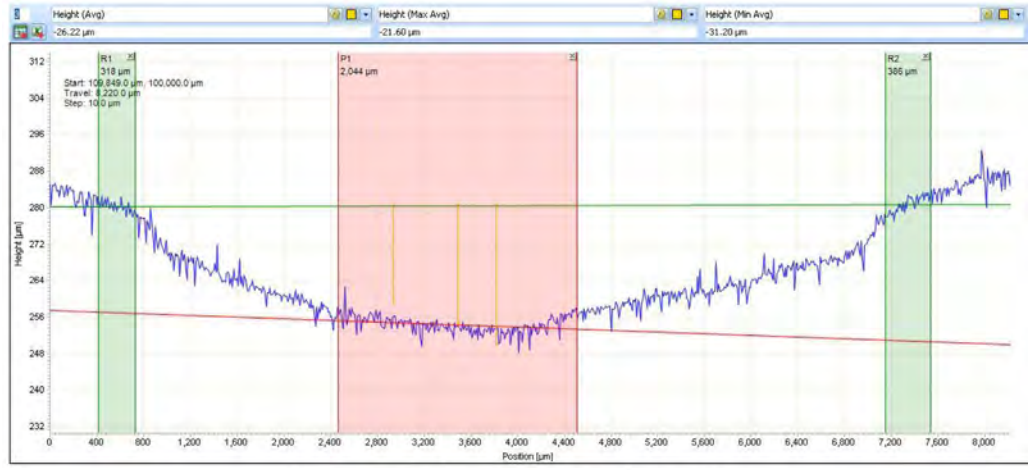

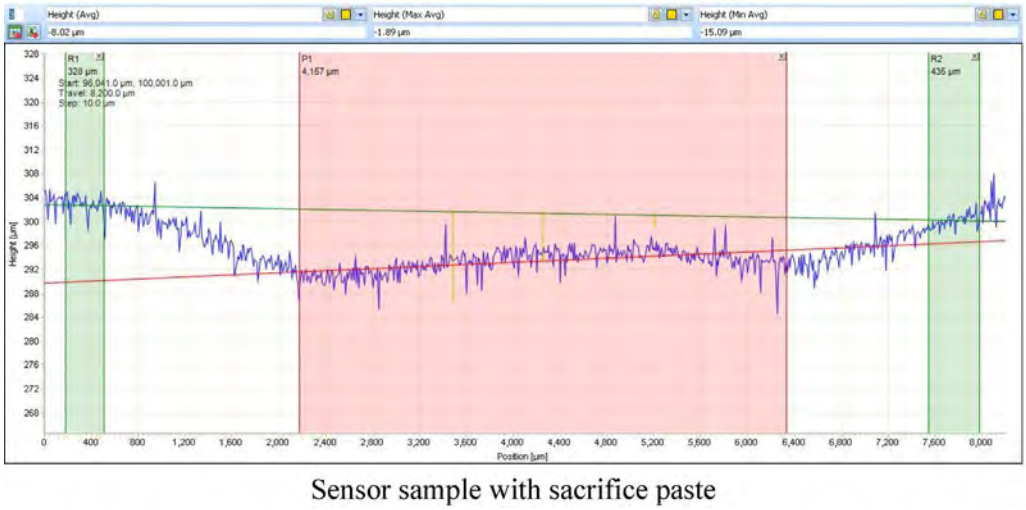

Fig. 3. Comparison of finished sensor samples with and without sacrifice paste.

results in the change of the sensor's resonant frequency. So the modeling of the structure is mainly about the theoretical deduction of the relations in between. The electromechanical model is applicable only on the premise that such assumptions are presumed:

1. the inductance of the sensor is a constant.
2. the pressure-defection model is based on thin plate theory and small defection theory.
3. the pressure-loaded membrane has a perfect surface flatness and with no residual strain is present in.

The schematic diagram of the sensor's electromechanical model is presented in Fig. 6a represents the length of the square capacitor cavity, t_g is the distance between the membranes, t_m thickness of the membrane. So the center defection d_0 of the membrane is given by [13]

$$d_0 = \frac{0.00126Pa^4 \times 12(1-\nu^2)}{E(2t_m)^3} \tag{2}$$

where P is the uniformly applied pressure load ranging from 0 MPa to 0.36 MPa, E the Young's modulus, P the pressure applied and ν is the Poisson's ratio. t_m is the thickness of the membrane.

As shown in Fig. 6, the capacitor C_s of the sensor, whose metal electrodes are separated by membranes and cavity, is a function of d_0 [3]

$$C_s = C_0 \frac{\tanh^{-1}\left(\sqrt{2d_0/(t_g + (4t_m/\varepsilon_r))}\right)}{\sqrt{2d_0/(t_g + (4t_m/\varepsilon_r))}} \tag{3}$$

C_0, the capacitance at zero pressure, is given by

$$C_0 = \frac{\varepsilon_0 a^2}{t_g + (4t_m/\varepsilon_r)} \quad \text{(square membrane)} \tag{4}$$

where a is the length of the square electrode, t_g the depth of the cavity and t_m the thickness of the membrane, ε_0, ε_r are the free space permittivity and relative dielectric constant respectively.

With the parameter of the sensor presented in Table 1, we can draw a theoretical pressure-defection diagram, thus the pressure–capacitance diagram, as shown in Figs. 7 and 8.

The square planar spiral inductance of the sensor can be derived from the expression which is a simple modification of the original Wheeler formula [14]:

$$L_S = K_1 \mu_0 \frac{n^2 d_{avg}}{1 + K_2 \rho} \tag{5}$$

where coefficients K_1 and K_2 are layout dependent and shown in Table 3, μ_0 is permeability of vacuum and n the number of

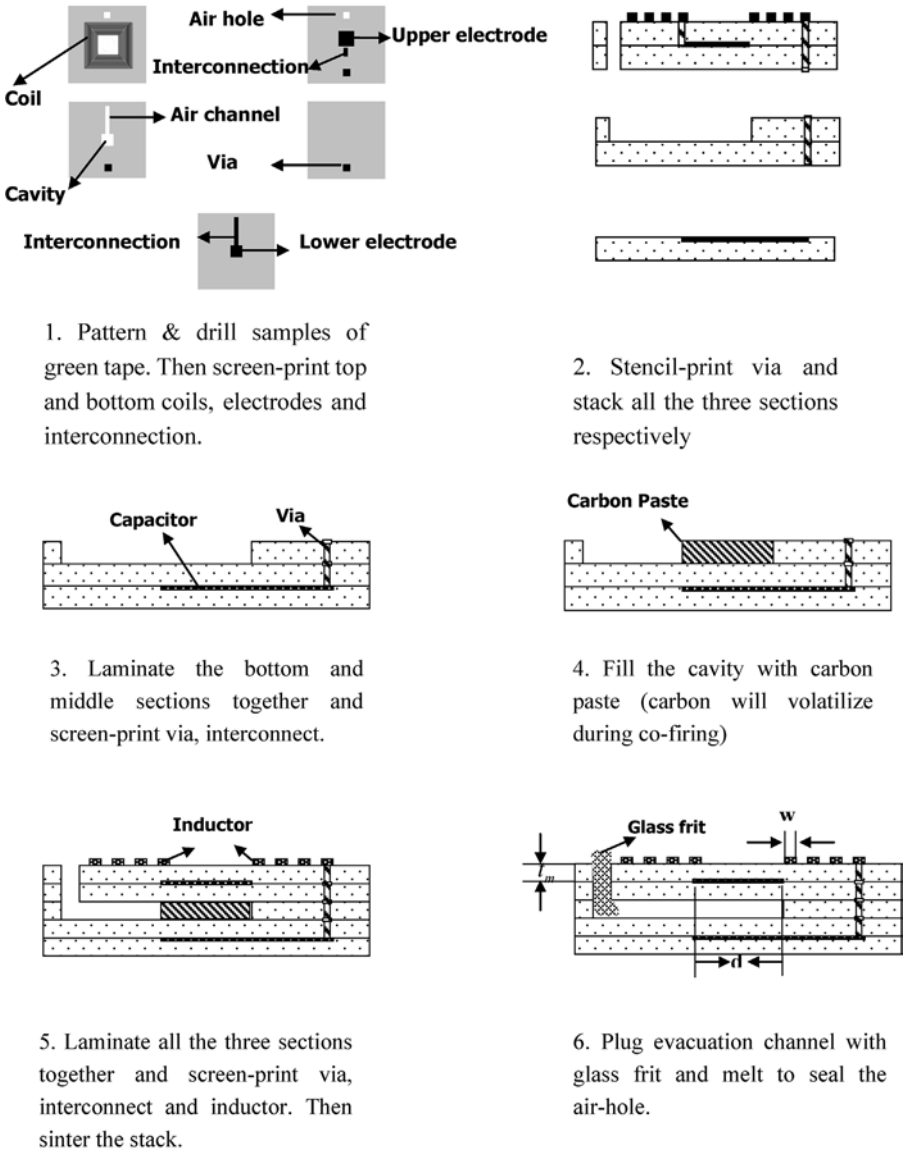

Fig. 4. Process flow of the sensor (the layer thickness t_m is 100 μm, the width of inductor coil w and the space between neighbor coils are both 0.15 mm, the side length of the square capacitor plate d is 7 mm).

coil turns, the average diameter $d_{avg} = ((d_{in} + d_{out})/2)$, ρ is the fill ratio defined as $\rho = ((d_{out} - d_{in})/(d_{out} + d_{in}))$, where d_{in} is the inner diameter and d_{out} the outer.

The theoretical inductance is calculated as 6.43 μH from the parameter demonstrated in Table 3, then the pressure–frequency diagram is obtained when we take the earlier deductions together, which is shown in Fig. 9.

4. Measurements and results

The harsh working environment determines that the measurement of the sensor has to be a contactless way, so a wireless measurement model, where the sensor coil being coupled to a reader coil, is established. As shown in Fig. 10, through the coupling of the reader coil and sensor coil, the signal of the pressure variation is translated to that of frequency variation, then transmitted to the antenna which consists of a LC resonant circuit.

As the impedance of the antenna is given by [15]

$$Z = R_1 + j2\pi L_1 \left(1 + \frac{k^2 (f/f_0)^2}{1 + j(1/Q)(f/f_0) - (f/f_0)^2}\right) \quad (6)$$

where R_1 is the ohmic series resistance of the reader coil and L_1 the inductance of the reader coil, f_0 the sensor's resonance frequency, k the coupling coefficient, Q the sensor's quality factor. The variation of the sensor's resonance frequency is then indicated by that of the antenna's impedance characteristics, we mainly take the impedance's magnitude and phase properties into consideration.

Fig. 11 is the magnitude and phase of the impedance (at zero pressure) measured by Agilent E4991A impedance analyzer, Fig. 11a is the impedance's characteristic of the reader coil before being coupled by the sensor, and Fig. 11b that after. Due to the sensor's coupling effect, the phase and magnitude of the antenna's impedance changed significantly. At the resonance frequency, the

Table 3
Coefficients K_1, K_2.

Layout	K_1	K_2
Square	2.34	2.75
Hexagonal	2.33	3.82
Octagonal	2.25	3.55

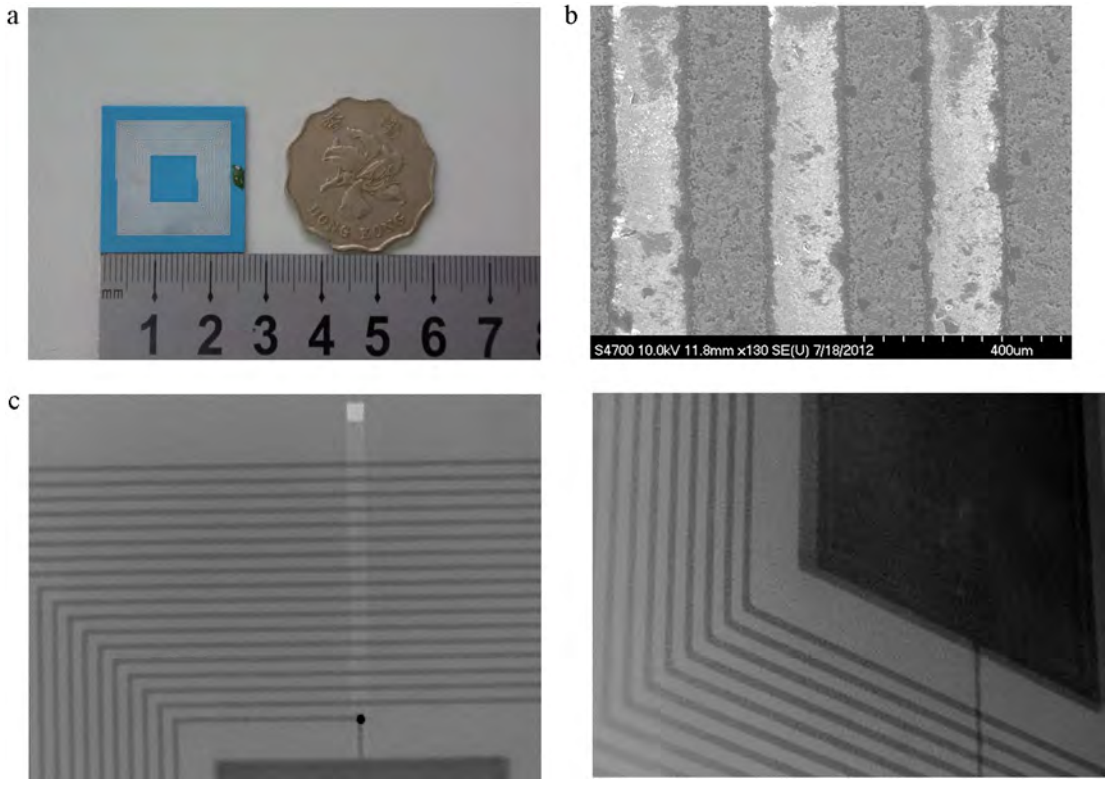

Fig. 5. (a) Sensor sample. (b) SEM image of the surface inductor coils. (c) X-ray images of air channel and capacitor electrodes.

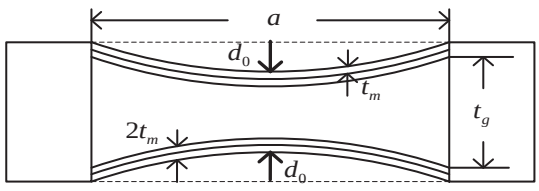

Fig. 6. Sensor's electromechanical model.

phase of impedance has a 180° turnover where the phase minimum f_{min} occurs, and the magnitude of impedance reaches a maximum. The tested sensor's f_{min} is 19.62 MHz at zero pressure, as the pressure applied increases, both f_{min} and $|Z_{max}|$ would shift left on the frequency axis.

The Taylor expansion of the phase minimum f_{min} is given by [1]

$$f_{min} = f_0 \left(1 + \frac{k^2}{4} + \frac{1}{8Q^2}\right) \tag{7}$$

Constant k and Q is measured by the impedance analyzer, and the pressure–resonance frequency chart is established.

The sensor and antenna are put into a closed vessel for measurement, where nitrogen gas is pumped through GE PACE 5000 pressure controller to make sure of a controllable uniform pressure condition, pads are placed on the surface of the vessel, which is connected to the antenna on one side for signal collecting, and Agilent E4991A impedance analyzer on the other side for signal reading. The whole measurement platform is shown in Fig. 12.

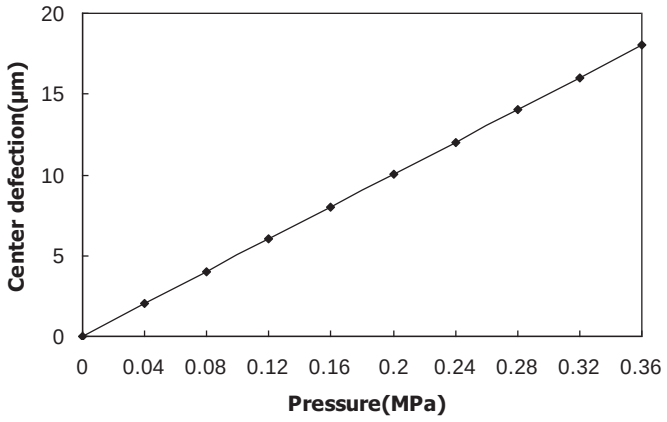

Fig. 7. Defection versus applied pressure.

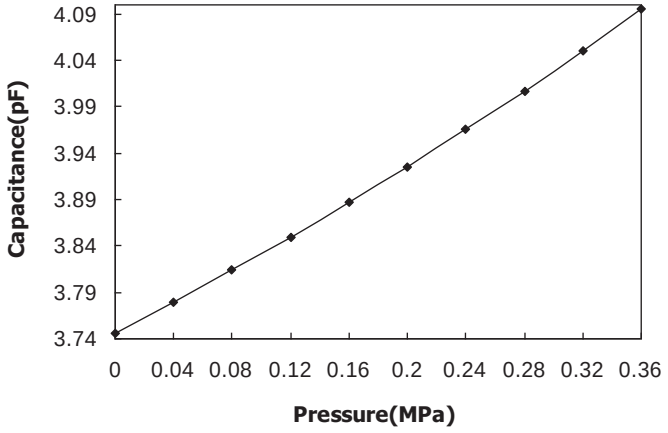

Fig. 8. Capacitance versus applied pressure.

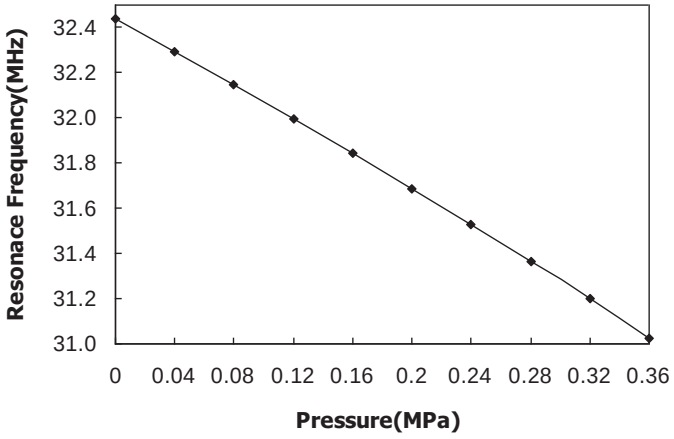

Fig. 9. Resonance frequency versus applied pressure.

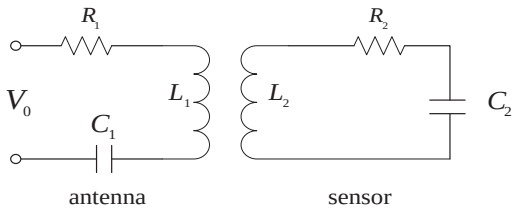

Fig. 10. Coupling model.

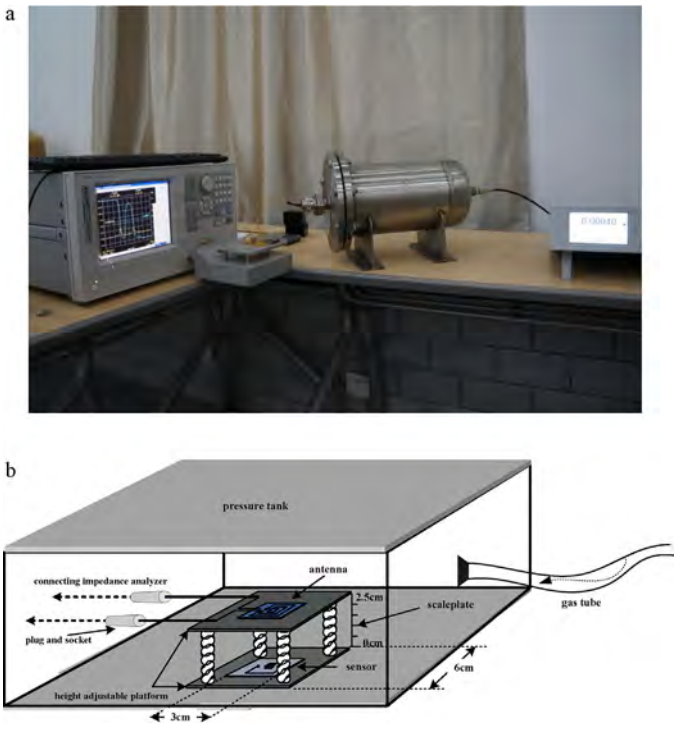

Fig. 12. (a) Measurement platform. (b) Measurement system setup.

The pressure applied ranges from 0 to 0.36 MPa, Fig. 9 is pressure–frequency relational graph (Fig. 13).

As we can see from the graph, the resonance frequency of the sensor is 18.94 MHz, which is 42% lower than theoretical value, the measured inductance of antenna coil is 7.54 μH, which contributes only 8% of the frequency discrepancy comparing to the theoretical 6.43 μH, thus the discrepancy of frequency is mainly caused by that of the capacitance between theoretical and experimental value. The possible factors are concluded as following: (1) the capacitor electrodes are larger than the cavity. The superfluous parts of the electrodes, which are sandwiched between ceramic layers but not ceramic layer and vacuum as the overlap parts, distribute a lot to the sensor's capacitance because of the larger dielectric constant of ceramic compared to vacuum. (2) Though the

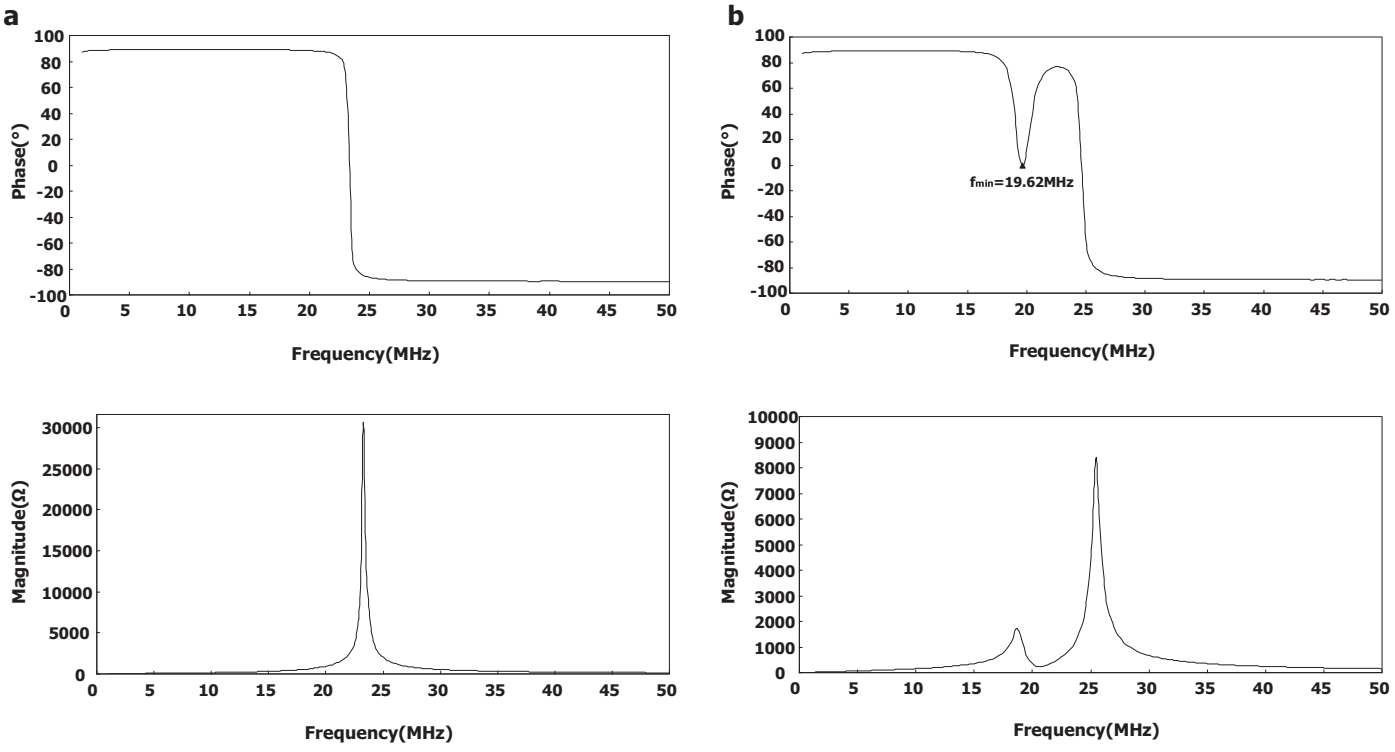

Fig. 11. (a) Phase and magnitude of the impedance before being coupled. (b) Phase and magnitude of the impedance after being coupled.

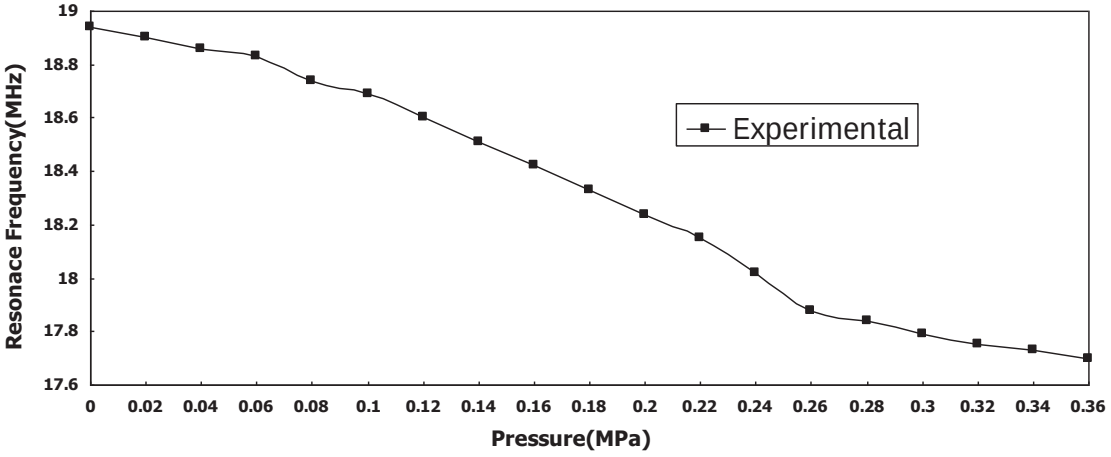

Fig. 13. Experimental results.

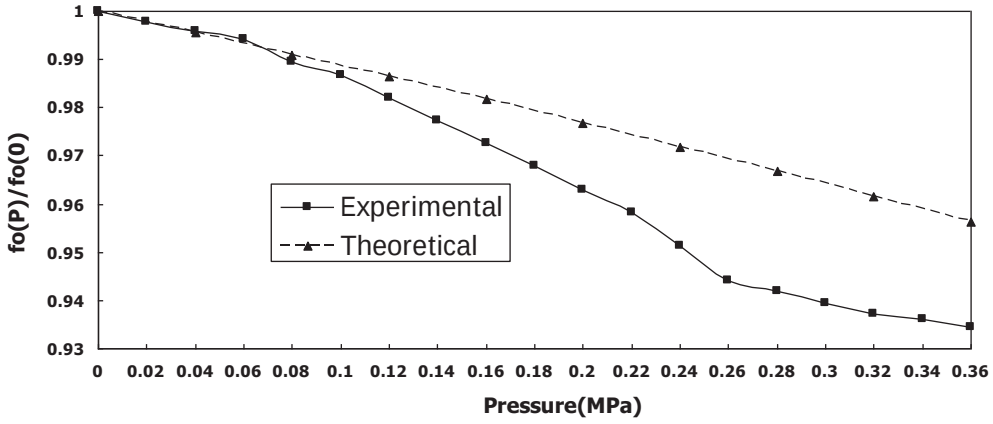

Fig. 14. Normalized comparison of experimental and theoretical results.

sacrifice paste is stuffed into the embedded cavity, there is still a certain collapse or pre-defection of the sensitive membrane during manufacture process (about 10 μm), which shortens the distance between capacitor electrodes, then increases the capacitance. Both effects would decrease the resonant frequency by increasing the capacitance.

Fig. 14 is the normalized comparison between theoretical and experimental resonant frequency versus applied pressure, from which we can clearly see that the tendency of the experimental curve is in good accordance with the theoretical one, the sensor's sensitivity is as high as −344 kHz/bar, which is more than 2 times of that of Georgia Tech's team, 14 times of Novi Sad'.

The improvement of the sensitivity mainly results from the favorable flatness of the sensitive membrane, as obtained from experiment, the sensitivity of sensors with nearly 70 μm deformation is only −20 kHz/bar around.

Fig. 15 presents the sensor's resonant frequency behavior as a function of temperature, from which we can see that from room temperature to 500 °C the average slope is −1.85 kHz/°C, and −10.545 kHz/°C from 500 °C to 600 °C, the possible factors that lead to the degeneration may be as following: (1) the relative permittivity of ceramic would vary as temperature rises, which would influence the capacitance; (2) the sensor's LC circuit performance would be affected by the temperature, the change of capacitance or inductance would lead to variation of resonant frequency; (3) as the high temperature measurement platform is relatively enclosed, the rise of temperature would cause the variation of atmospheric pressure, which equals the extra pressure loaded to the sensor, so the frequency is decreased. For future high-temperature application, the parasitic temperature dependence needs to be compensated.

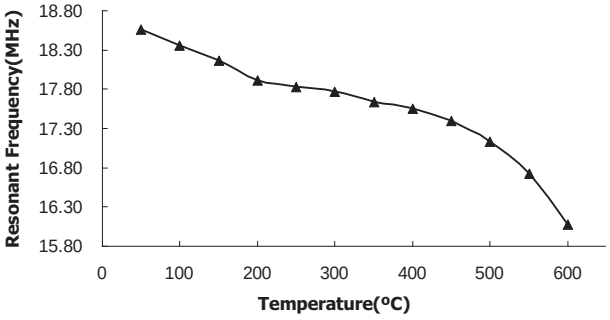

Fig. 15. Resonant frequency versus temperature.

5. Conclusions

A wireless high-temperature capacitive pressure sensor based on LTCC (low temperature co-fired ceramic) technology is realized, a unique sacrifice paste process is introduced, a wireless measurement model, where the sensor coil is coupled to a reader coil, is established, and a barometric-pressure measurement platform is built.

Sensor samples are been tested under uniform gas pressure, where an excellent performance is shown, the sensor's sensitivity reaches as high as −344 kHz/bar.

As the sensor's sensitivity is decided by the capacitor's sensitivity, future optimization of cavity and the membrane will greatly improve the sensor's sensitivity, as LTCC materials, like Al_2O_3, is greatly limited by the bad flexibility when serving as membranes, we would like to try a better substitute material such as Zr_2O_3.

Acknowledgments

The authors would like to thank Senior Engineers: Jun Li, Youcheng Li, and Yingling Wang from the 2nd research institute of China electronics technology group corporation, Taiyuan, China, for useful technical advice.

The research was supported by the National Basic Research Program of China (973 Program) under the Grant of No. 2010CB334703. Additionally, the research was also supported by National Natural Science Foundation of China under Grant of No. 51075375.

Appendix A. Supplementary data

Supplementary data associated with this article can be found, in the online version, at http://dx.doi.org/10.1016/j.sna.2013.04.007.

References

[1] M.A. Fonseca, J.M. English, M. Arx, M.G. Allen, Wireless micromachined ceramic pressure sensor for high-temperature applications, Journal of Microelectromechanical Systems 11 (August (4)) (2002) 337–343.
[2] J. English, M.G. Allen, Wireless micromachined ceramic pressure sensors, in: Proc. Twelfth IEEE Microelectromechanical Systems Conf., 1999, pp. 511–516.
[3] M.A. Fonseca, Polymer/ceramic wireless MEMS pressure sensors for harsh environments: high temperature and biomedical applications, Georgia Institute of Technology 2007, Dissertation Abstracts International, Vol. 68-12, Section: B, 8247; 270 p.
[4] E.D. Birdsell, J. Park, M.G. Allen, Wireless ceramic sensors operating in high temperature environment, in: 40th ALAA/ASME/SAE/ASEE Joint Propulsion Conference, Fort Lauderdale, FL, July 2004, 2004.
[5] G. Radosavljevic, L.J. Živanov, W. Smetana, A. Maric, M. Unger, L. Nad, A wireless embedded resonant pressure sensor fabricated in the standard LTCC technology, IEEE Sensor Journal 9 (December (12)) (2009) 1956–1962.
[6] G. Radosavljevic, W. Smetana, A. Mari, L.J. Živanov, M. Unger, G. Stojanovi, Micro force sensor fabricated in the LTCC technology, in: Proc. 27th International Conference on Microelectronics (MIEL 2010), Niš, Serbia, 16–19 May, 2010.
[7] Y. Hezarjaribi, M.N. Hamidon, S.H. Keshmiri, A.R. Bahadorimehr, Capacitive pressure sensors based on MEMS, operating in harsh environments, in: 2008 IEEE International Conference on Semiconductor Electronics, 2008.
[8] C.B. Sippola, C.H. Ahn, A hermetic thick film screen-printed ceramic cavity for harsh environment sensing applications, IEEE Transactions on Components and Packaging Technologies 30 (September (3)) (2007) 439–443.
[9] M.G.H. Meijerink, E. Nieuwkoop, E.P. Veninga, M.H.H. Meuwissen, M.W.W.J. Tijdink, Capacitive pressure sensor in post-processing on LTCC substrates, Sensors and Actuators A 123/124 (2005) 234–239.
[10] H. Birol, T. Maeder, P. Ryser, Processing of graphite-based sacrificial layer for microfabrication of low temperature co-fired ceramics (LTCC), Sensors and Actuators A 130/131 (2006) 560–567.
[11] L.E. Khoong, Y.M. Tan, Y.C. Lam, Overview on fabrication of three-dimensional structures in multi-layer ceramic substrate, Journal of the European Ceramic Society 30 (2010) 1973–1987.
[12] www.dupont.com
[13] S.P. Timoshenko, S. Woinowsky-Krieger, Theory of Plates and Shells, McGraw-Hill, NYC. US, 1959.
[14] S.S. Mohan, M. Hershenson, S.P. Boyd, T.H. Lee, Simple accurate expressions for planar spiral inductances, IEEE Journal of Solid-State Circuits 34 (October (10)) (1999) 1419–1424.
[15] R. Nopper, R. Has, L. Reindl, A wireless sensor readout system – circuit concept, simulation, and accuracy, IEEE Transactions on Instrumentation Measurement 60 (August (8)) (2011) 2976–2983.

Biographies

Jijun Xiong received his BSc and MSc degrees in electrical engineering from North Universtiy of China in Shanxi, China, in 1993 and 1998, and PhD degree in Precision Instruments and Mechanology from Tsinghua University in Beijing, China. in 2003. His research interest is in the fields of measurement and MEMS.

Ying Li received his BS degrees from Suzhou University, China, in 2009, He is currently in the graduate program at North University of China to pursue his MS degree. His research interest is in MEMS sensors.

Ting Liang received his BS degrees from Tianjin University, China, in 2002, MS and PhD degrees in Microelectronics and solid electronics from Beijing University Of Technology, China, respectively in 2005 and 2007. His research interest is in MEMS sensors.